Biomaterials Science

Magneto Mitochondrial Dysfunction Mediated Cancer Cell Death Using Intracellular Magnetic Nano-Transducers

Journal:	*Biomaterials Science*
Manuscript ID	BM-ART-03-2021-000419.R1
Article Type:	Paper
Date Submitted by the Author:	20-May-2021
Complete List of Authors:	Park, Wooram; The Catholic University of Korea, Center for Photomedicine, Department of Biotechnology Kim, Seok-Jo; Northwestern University Feinberg School of Medicine Cheresh, Paul; Northwestern University Feinberg School of Medicine Yun, Jeanho; Dong-A University Lee, Byeongdu; Argonne National Laboratory, X-ray Sciences Division; Kamp, David; Northwestern University Feinberg School of Medicine Kim, Dong-Hyun; Northwestern University Feinberg School of Medicine, Department of Radiology

Magneto Mitochondrial Dysfunction Mediated Cancer Cell Death Using Intracellular Magnetic Nano-Transducers

Wooram Park,[1,2†] Seok-Jo Kim,[3,4,5†] Paul Cheresh,[3,4] Jeanho Yun,[6] Byeongdu Lee,[7] David W. Kamp,[3,4] and Dong-Hyun Kim[1,8,9]*

[1]Department of Radiology, Feinberg School of Medicine, Northwestern University, Chicago, Illinois 60611, United States
[2]Department of Biomedical-Chemical Engineering, The Catholic University of Korea, 43 Jibong-ro, Wonmi-gu, Bucheon-Si, Gyeonggi 14662, Republic of Korea
[3]Department of Medicine, Division of Pulmonary & Critical Care Medicine, Jesse Brown VA Medical Center, Chicago, Illinois 60612, United States
[4]Department of Medicine, Northwestern University Feinberg School of Medicine, Chicago, Illinois 60611, United States
[5]Division of Rheumatology, Department of Internal Medicine, University of Michigan, Ann Arbor, MI 48109, United States
[6]Department of Biochemistry, College of Medicine, Dong-A University, Busan 49201, Republic of Korea
[7]X-Ray Science Division, Argonne National Laboratory, Argonne, IL, 60439 United States
[8]Department of Biomedical Engineering, McCormick School of Engineering, Evanston, IL 60208, United States
[9]Robert H. Lurie Comprehensive Cancer Center, Northwestern University, Chicago, Illinois 60611, United States

[†]These authors contributed equally to this work.

***CORRESPONDING AUTHOR**

E-mail: dhkim@northwestern.edu (Prof. Dong-Hyun Kim)

KEYWORDS: Mitochondrial Targeting; Iron Oxide Nanoparticles; Magnetic Nano-transducers; Image-guided Therapy; Mitochondrial Dysfunction; Cancer Treatment

Abstract

Mitochondria are crucial regulators of the intrinsic pathway of cancer cell death. The high sensitivity of cancer cells to mitochondrial dysfunction offers opportunities for emerging targets in cancer therapy. Herein, magnetic nano-transducers, which convert external magnetic fields into physical stress, are designed to induce mitochondrial dysfunction to remotely kill cancer cells. Spindle-shaped iron oxide nanoparticles were synthesized to maximize cellular internalization and magnetic transduction. The magneto-mechanical transduction of nano-transducers in mitochondria enhances cancer cell apoptosis by promoting a mitochondrial quality control mechanism, referred to as mitophagy. In the liver cancer animal model, nano-transducers are infused into the local liver tumor via the hepatic artery. After treatment with a magnetic field, *in vivo* mitophagy-mediated cancer cell death was also confirmed by mitophagy markers, mitochondrial DNA damage assay, and TUNEL staining of tissues. This study is expected to contribute to the development of nanoparticle-mediated mitochondria-targeting cancer therapy and biological tools, such as magneto-genetics.

Introduction

Controlling the temporal and spatial signaling processing of cellular organelles through specific physical stimuli has been of great interest in manipulating the biological functions of cells.[1, 2] Chemical agents and opto-genetics have been studied as tools for regulating various cell signals. However, chemical strategies delay the regulation of cellular function because of their slow pharmacokinetics, and optical methods have limited the control of cellular functions in deep tissues owing to the low tissue permeability of light.[3] Therefore, magnetic field stimulation has been considered as a next-generation cell perturbation technology.[3-5] Magnetic nanoparticles in the magnetic cell perturbation techniques have been attracting attention because they can be targeted to disease sites with high efficacy, and transduce one physical stimuli into another type of stimuli.[2] For example, magnetic nanoparticles facilitate the transduction of external magnetic fields into mechanical forces or heat energy.[4-10] Owing to the tissue-penetrating nature of magnetic fields, combining magnetic nanoparticles and controlled external magnetic fields has extensive potential for the remote control of cell signaling for specific purposes such as cancer therapy for treating specific diseased cells in deep tissues. Inspired by magneto-genetics, opto-genetics, and cell perturbation technology, we report a magneto-mitochondrial perturbation technique to treat cancer cells using mitochondria-targeted magnetic nano-transducers.

Cancer cells are characterized by limited proliferative potential and impaired apoptosis owing to the dysregulation of multiple cellular signaling mechanisms.[11] Various therapeutic approaches that target signaling pathways or metabolic processes that are preferentially dysregulated in cancer cells are being developed for cancer treatment.[12] Otto Warburg reported that defects in

mitochondrial respiration inducing unusually enhanced glycolysis and is an underlying basis for cancers.[13] Since then, the mitochondria, which are central metabolic organelles, have emerged as a new target for cancer therapy. Recent studies have confirmed that multiple hallmarks of cancer cells, including excessive proliferation, insensitivity to anti-growth signals, resistance to apoptosis, enhanced anabolism, and decreased autophagy, are linked to mitochondrial activity in the cells.[12, 14-16] Indeed, cancer cellular mitochondrial biogenesis and quality control are often significantly upregulated.[17] The regulation of the mitochondrial function may offer opportunities to selectively induce cancer cell apoptosis and inhibit tumor progression to malignancy, where one may take advantage of the acute sensitivity of cancer cells to mitochondrial dysfunction.[18] Thus, the development of a new concept for mitochondrial-targeted cancer therapy is of great interest.

Mitochondrial porin channels and receptors located on the outer mitochondrial membrane (OMM) and inner mitochondrial membrane (IMM) are essential for mitochondrial function and cell apoptosis.[19, 20] If the mitochondrial membrane receptors or porins on the OMM/IMM are stimulated or damaged by external stimuli, mitochondrial-related cellular signaling can be easily perturbed, initiating potential mitophagy or cell apoptosis.[20-23] We hypothesized that mitochondria targeting magnetic nano-transducers, converting external magnetic fields into physical stress, induce mitochondria-mediated cell death signaling (**Figure 1a**). Particularly, we found that significant cancer cell death was attributed to excessive mitophagy induced by magnetic nano-transducers. To the best of our knowledge, this is the first strategy for cancer cell death through the induction of mitophagy-mediated cell death signaling by nano-transducers under remote-controlled magnetic fields, without any chemical agents. Our results may have an impact on cellular biology and nano-bio interfaces and open a new horizon in cancer treatment and various

areas.

Results and discussion

The magnetic nano-transducers used in this study were designed using spindle-shaped iron oxide nanoparticles to maximize cellular internalization[24, 25] and magnetic transduction[26]. The as-designed nano-transducers were synthesized in two steps.[26, 27] First, spindle-shaped FeOOH nanoparticles were prepared by the hydrolysis of $FeCl_3$ (**Figure S1 and Table S1,** Supporting Information). The prepared FeOOH nanoparticles were converted to a magnetite (Fe_3O_4) phase in oleylamine at 200 °C.[26] Oleylamine acted as both a reducing agent and surfactant during the synthetic process. The reduction process was optimized through a series of experiments. Reduction for 4 h could form optimum nanoparticles; however, the nanoparticles were aggregated at a reduction time of 12 h (**Figure S2,** Supporting Information). The synthesized magnetic nano-transducers were approximately 40 nm in length and 15 nm in width with an aspect ratio of approximately 2.5 (**Figure 1b-1e**). For bio-applications, the ligand (*i.e.,* oleylamine) on the nanoparticle surface was ligand-exchanged with mitochondria-targeting polymeric ligands (*i.e.,* polyethylene glycol (PEG) modified with triphenylphosphine (TPP))[28] and 3,4-dihydroxyphenylacetic acid (DOPAC) (**Figure 1f and Figure S3,** Supporting Information)[29]. Successful surface modification was confirmed by Fourier transform infrared (FT-IR) analysis (**Figure S4,** Supporting Information). The zeta potential of the nanoparticles was approximately +30 mV because of the TPP on the surface of the nanoparticles. The TPP-coated nano-transduces showed stable colloidal stability in the aqueous phase for one week (data not shown). The

synthesized nano-transducers exhibited superparamagnetic properties (**Figure 1g**).[26] To examine the magneto-mechanical transduction behavior of the nano-transducers upon magnetic field application, small-angle X-ray scattering (SAXS) was used (**Figure 1h and i**). The nanoparticles were dispersed in an artificial biomimetic solution of glycerol and water (70:30 w/w),[30] which is an environment of viscosity similar to the environment in an actual cell, and a magnetic field (10 Oe) was applied. The nanotransducers were effectively responsive to an external magnetic field of 2 Hz. Extended exposure to the magnetic field may connect the nanoparticles, resulting in a delay of magnetic responsive movement; however, the magnetic responsive movement was observed during the 30-minute measurement period.

To confirm the intracellular internalization of the nanoparticles, bio-transmission electron microscopy (TEM) was used in liver cancer cells (McA-RH7777). As shown in **Figure 2**, nano-transducers were introduced into the cells via an endocytosis mechanism. Remarkably, the scene in which the nano-transducers escaped the endosome was captured by TEM (**Figure 2a and b**). This is because the nano-transducers can disrupt the endo-lysosomal membrane and be internalize into the cytosol. In previous studies,[31-33] TPP-modified nanoparticles successfully targeted the intracellular mitochondria. Finally, a confocal microscope (**Figure 2c and d**) and an electron microscope (**Figure 2e**) were used to confirm the mitochondrial targeting of the nano-transducers. Many nanoparticles could be effectively targeted to the mitochondria because the cationic TPP molecules on the surface of the nanoparticles can target the mitochondrial membrane potential.[34, 35] These results suggest that the developed nano-transducers were effectively targeted to the mitochondria, which is one of the major intracellular organelles, after being internalized through endocytosis in liver cancer cells.

Subsequently, we aimed to understand the biological significance of the mitochondria-targeted nano-transducers in liver cancer cell death exposed to external magnetic fields. The cell viability was measured after treatment with various concentrations of nano-transducers using an MTT assay. The cell viability of McA-RH7777 exhibited a clear reduction across 150 (98.0± 1.8%) to 500 (66.9 ± 9.9%) μg/mL of the nano-transducers dose range **(Figure 3a)** and the highest anti-proliferative effect after 24 h exposed with a well-resonated frequency of 2.0 Hz magnetic field for 15 minutes **(Figure 3b).** Optimized frequency with cell viability is also proving the magneto-mechanical force is effectively transferred from nano-transducers to the cells.[36, 37] Based on these results, further *in vitro* experiments were conducted at concentrations lower than 200 μg/mL of nano-transducers with a magnetic field frequency of 2.0 Hz. Additionally, the LIVE/DEAD cell vitality assay showed lower survival of the nano-transducer-treated McA-RH7777 cells with external magnetic fields compared to the untreated group **(Figure 3c)**. Mitochondrial DNA damage-mediated apoptosis was also augmented in the nano-transducer-exposed McA-RH7777 cells under magnetic field conditions (**Figure 3d and e)**, suggesting a triggering mitochondrial damage response.[38]

Thus, we were interested in understanding the effect of mitochondria-targeted nano-transducers on the mitochondria for hepatoma cell death. As mentioned above, mitochondria play a multifunctional role in malignant tumor progression, and targeting mitochondria provide therapeutic opportunities.[39] The mitochondrial damage-regulated autophagy modulator (DRAM) can induce apoptosis in HCC cells through mitophagy, which promotes DRAM-mediated autophagy alongside PI3K/AKT inhibition.[40] Mitophagy, known as selective autophagy of the mitochondria, is an important mitochondrial quality control mechanism that eliminates damaged

mitochondria.[41] In the initiation of mitophagy, PTEN-induced kinase 1 (PINK1) and Parkin accumulate on damaged mitochondria; the stabilization of PINK1 and the translocation of Parkin are required on the OMM, especially for the translocase of the outer membrane (TOM) complex.[41-44] Our data showed that the levels of the mitochondrial protein TOM 20 were decreased in a time-dependent manner in the nano-transducer-treated McA-RH7777 cells with magnetic fields, whereas the mitochondrial translocase of the inner membrane 23 (TIM 23) was not affected (**Figure 4a** and **Figure S5, Supporting Information**). This indicates damage to the OMM rather than the IMM by nanoparticles perturbed by the magnetic field. Additionally, an increase in PINK1 and Parkin expression levels was observed in the McA-RH7777 cells under the same conditions, suggesting that Parkin promotes the degradation of OMM proteins, causing mitophagy.[45] It is known that Parkin ubiquitinates mitochondrial substrates to recruit p62, which interacts with light chain 3 (LC3-I) to form autophagosomes for mitochondrial quality control, and LC3 is converted to a lipidated form by the phosphatidylethanolamine conjugation of LC3 (LC3-II).[46, 47] To characterize the dynamics of mitochondrial turnover by autophagy (mitophagy), our data addressed that the conversion of LC3-I to LC3-II was increased in the nano-transducer-treated McA-RH777 cells with magnetic fields in a time-dependent manner (**Figure 4a**). However, the treatment of the nano-transducers with magnetic fields reduced the p62 level in the McA-RH7777 cells, which is typically degraded in cells with autophagic flux.[48] Furthermore, we monitored the induction of mitophagy in the McA-RH7777 cells through mt-Keima, a ratiometric pH-sensitive fluorescent protein targeted to mitochondria and resistant to lysosomal proteases.[49, 50] The intrinsic pH difference of mitophagy allows the ratio of green (*i.e.,* neutral mitochondria) to red (*i.e.,* acidic mitophagy) fluorescence to reflect the underlying level of mitophagy.[49, 50] In the mt-Keima assay,

as shown by confocal microscopy, the magnetic fields caused an increase in the mitophagy index in the McA-RH7777 cells treated with nano-transducers (**Figure 4b**): red mt-Keima punctate structures, an indicator of mitochondrial mitophagic process, were significantly increased when the nano-transducers were treated with magnetic fields, which indicates an increase in mitophagy in the cancer cells. Protonophore-carbonyl cyanide 3-chlorophenylhydrazone (CCCP) and oligomycin were used as positive control groups to induce mitophagy. The confocal image of the positive control group was similar to that of the McA-RH7777 cells treated with both transducers and magnetic fields. These results demonstrate that the mitochondrial damage caused by the nano-transducers under external magnetic field conditions induces apoptosis of cancer cells related to the mitophagy mechanism. Several recent studies have reported that the deregulation of the mitophagy process that maintains cellular energy homeostasis and function[51] is linked to cancer cell death[18, 52, 53] and eliminating mtDNA limits tumorigenesis[54]. Therefore, it is reasonable to target mitophagy as a potential therapeutic target. Moreover, overwhelming evidence has shown a fundamental role of mitophagy in many physiological events, from development to aging; its deregulation contributes to many diseases, including neurodegenerative diseases and immunological disorders.[51, 53, 55] Regulating mitophagy as a therapeutic strategy in both healthy and cancer cells will provide promising opportunities for various applications.

Finally, we tested the magneto mitochondrial dysfunction-mediated cancer cell death using magnetic nano-transducers in HCC rat models. The HCC animal models were generated by orthotopic transplantation, and the magnetic nano-transducers were locally injected into the hepatic artery using X-ray DSA and magnetic resonance imaging (MRI) image-guided transcatheter intra-arterial infusion.[56, 57] MRI was used to confirm that the infused magnetic nano-

transducers were targeted for liver cancer. The accumulation of large amounts of nano-transducers around the tumor site was confirmed by T_2 MR imaging (**Figure 5a and b**). After the nano-transduces were injected, magnetic fields generated by an external electronic magnet were carefully applied to the location of the liver tumor region using ultrasound and MRI imaging (**Figure 5c**). Such image-guided nanoparticle infusion and the application of external magnetic fields could minimize side effects in normal tissues. The immunohistochemistry data showed that the apoptosis of the liver cancer cells was significantly increased when a magnetic field was applied (**Figure 5d and e**). When the tumor tissues were collected and analyzed, it was confirmed that mitochondrial DNA damage was significantly increased when the nanoparticles were treated, and the magnetic field was applied (**Figure 5f**), and the rate of apoptosis was also increased (**Figure 5g).** The western blot analysis of the tumor tissues revealed a decrease in TOM20 and an increase in PINK1 upon treatment with nano-transducers, and magnetic fields were applied, similar to the results of the *in vitro* experiments **(Figure 5h**). Overall, in the animal experiments, it was found that when the nano-transducers were treated with a magnetic field, the cancer cells could induce apoptosis-related mitochondrial dysfunction, as demonstrated by the *in vitro* test. Detailed *in vivo* safety studies of magnetic nano-transducers and further research using nanoparticles conjugated with targeting ligands to minimize side effects of normal tissues are now clearly warranted.

Conclusions

In this study, we described a novel cellular control technique for remotely inducing cancer cell

death by damaging the mitochondria through intracellular magnetic nano-transducers under external magnetic fields. Spindle-shaped nano-transducers were synthesized by high heat treatment and coated with ligands capable of targeting intracellular mitochondria. It was confirmed that the technique effectively targeted mitochondria in cancer cells. Nano-transducers with a magnetic field induced apoptosis of cancer cells through mitochondrial damage by magneto-mechanical stress, which is related to the mitophagy mechanism. In the liver cancer animal model, the nano-transducers were infused into HCC using an interventional technique, and an external magnetic field was applied. It was also confirmed that magneto mitochondrial dysfunction using nano-transducers enhances apoptotic cell death in HCC. Molecular biology tools such as western blotting and mitochondrial DNA damage assay further proved that the *in vivo* results are consistent with the in vitro results and demonstrated that the magneto mitochondrial dysfunction by magnetic nano-transducers could ultimately kill cancer cells. This study is expected to contribute to the development of next-generation biological tools, such as the magnetogenetics and development of cancer therapy in nanotechnology through the spatial and temporal control of biological mechanisms.

Experimental Section

All reagents and solvents were obtained commercially and used without further purification. Iron(III) chloride anhydrous (≥99.99%), 3,4-dihydroxyphenylacetic acid (DOPAC), (4-carboxybutyl)triphenylphosphonium bromide (CTPP), oleylamine (70 %), poly (ethylene glycol) diamine (2 kDa, PEG-diamine), N,N- dicyclohexylcarbodiimide (DCC), rhodamine B isothiocyanate (RITC), tetrahydrofuran (THF), dichloromethane (DCM), and N, N-dimethylformamide (DMF) were Sigma–

Aldrich Co. (Milwaukee, WI, USA). Sulfo-N-hydroxysulfosuccinimide (S-NHS) was purchased from Thermo Fisher (Waltham, MA, USA).

Synthesis of TPP-PEG-DOPAC*:* This synthesis was performed with a slight modification of a previous report.[58] CTPP (44 mg), NHS (17 mg), and DCC (31 mg) were dissolved in DMSO (5 mL) and then stirred at 25 °C for 6 h. Subsequently, the mixture was added dropwise to DMSO containing PEG-diamine (200 mg) and stirred for another 8 h. Separately, DOPAC (17 mg) was activated with NHS (17 mg) and DCC (31 mg) in DMSO (5 mL) for 6 h. The activated DOPAC solution was then added to the CTPP and PEG mixtures. After reacting for an additional 6 h, TPP-PEG-DOPAC was dialyzed with a cellulose membrane (1 kDa, Spectrum Laboratories, Rancho Dominguez, CA, USA) in 0.01 N HCl solution. Finally, TPP-PEG-DOPAC was lyophilized after purifying a 0.22 μm cellulose filter (Whatman, Maidstone, UK).

Synthesis of RITC-PEG-DOPAC: RITC (54 mg) and PEG-diamine (200 mg) were dissolved in DMSO (5 mL) and then stirred at 25 °C for 6 h. Separately, DOPAC (17 mg) was activated with NHS (17 mg) and DCC (31 mg) in DMSO (5 mL) for 6 h. The activated DOPAC solution was then added to the RITC and PEG mixtures. After reacting for an additional 6 h, RITC-PEG-DOPAC was dialyzed with a cellulose membrane (1 kDa, Spectrum Laboratories, Rancho Dominguez, CA, USA) in 0.01 N HCl solution. Finally, RITC-PEG-DOPAC was lyophilized after purifying a 0.22 μm cellulose filter (Whatman, Maidstone, UK).

Synthesis of iron oxide nanospindles (IONS): The IONS were prepared by a two-step process. First, the β-FeOOH nanospindle was synthesized by the hydrolysis of $FeCl_3$ in an aqueous solution.[26, 59] In brief, 0.4 g of anhydrous $FeCl_3$ was dissolved in 40 mL water. The solution was added to a round-bottom flask and heated at 80 °C under mechanical stirring for 12 h to obtain uniform and spindle-shaped β-FeOOH nanoparticles. The particles were isolated by centrifugation (15,000 rpm, 15 min) and washed three times with deionized water (3 times) and twice with ethanol (2 times). The obtained nanoparticles were dried at room temperature for 24 h, and the as-prepared β-FeOOH nanospindles were reduced in oleylamine at 200

°C for transformation to magnetite (Fe_3O_4). Briefly, 0.1 g of β-FeOOH nanospindles and oleylamine (10 mL) were placed in a three-necked round-bottom flask. Under a nitrogen atmosphere, the solution was heated to 200 °C for 4 h. The final product was subjected to magnetic separation and washed several times with a mixture of hexane and acetone to remove any uncoordinated oleylamine.

Preparation of functionalized IONS: TPP-PEG-DOPAC (30 mg) was dissolved in 5 mL of THF. The above mixture was transferred to a 25 mL three-necked flask and heated to 50 °C under argon flow. Iron oxide nanospindles (10 mg) dissolved in THF (2 mL) were added to a 25 mL three-necked flask, and the mixture was incubated for 5 h at 50 °C. The functionalized IONS were collected by centrifugation (15,000 rpm, 10 min) and redispersed in ultrapure Millipore water (18.2 Ω).

Preparation of fluorescent (RITC)-labeled IONS: TPP-PEG-DOPAC (25 mg) and RITC-PEG-DOPAC (5 mg) were dissolved in 5 mL of THF. The above mixture was transferred to a 25 mL three-necked flask and heated to 50 °C under argon flow. Iron oxide nanospindles (10 mg) dissolved in THF (2 mL) were added to a 25 mL three-necked flask, and the mixture was incubated for 5 h at 50 °C. The fluorescent-labeled IONS were collected by centrifugation (15,000 rpm, 10 min) and redispersed in ultrapure Millipore water (18.2 Ω).

Small-angle X-ray scattering (SAXS) measurements: SAXS measurements were performed with an X-ray energy of 14 keV at the 12-ID-B station of the advanced photon source in the Argonne National Laboratory (Lemont, IL, USA). A Pilatus 2M detector was used to acquire scattering data with exposure times of 0.1 s. For the SAXS experiments, the magnetic nano-transducers (10 mg/mL) were dispersed in glycerol and water (70:30 w/w) in a 1.5 mm diameter glass capillary. The capillary was then placed horizontally on top of the electromagnet. SAXS data were collected while applying a sinusoidal voltage to the magnet with a function generator, which provided an external magnetic field of 10 Oe at 2 Hz. SAXS images acquired every 0.1 s were converted to 1D line intensity as a function of the azimuthal angle to monitor the orientation

of the nano-transducers or their assemblies. The 1D line data measured as a function of time were then stacked together and presented as the image shown in **Figure 1**.

Cell culture and cytotoxicity test: Rat McA-RH7777 cells were purchased from the American Type Culture Collection (ATCC CRL 1601, Rockville, MD, USA). The cells were cultured in Dulbecco's modified Eagle's medium (DMEM) supplemented with 10% fetal bovine serum (FBS). For serum starvation, the cells were incubated overnight with 0.5% FBS in DMEM. The cell viability test was performed using a 3-(4,5-demerthylthiazol-2-yl)-2, 5-diphenyltetrazolium bromide (MTT) assay using a Cell Proliferation Kit I (Roche, Mannheim, Germany) according to the manufacturer's recommendations. Briefly, 3×10^3 cells were seeded in 96-well culture plates with DMEM supplemented with 10% FBS. After 24 h, the medium was replaced with fresh medium, and the cells were incubated with different concentrations of nano-transducers (0-500 μg/mL) for 24 h. The electromagnetic field was then applied under various magnetic field frequency conditions (0.5 - 20.0 Hz, 10 Oe) for 15 min. Cell viability was determined by the MTT measurement of the optical density at a wavelength of 570 nm, with 750 nm as the reference wavelength. Live and dead cell assays were performed according to the manufacturer's instructions (Thermo Fisher Scientific Life Sciences, Rockford, IL, USA). McA-RH7777 cells were incubated with 150 μg/mL of nano-transducers for 24 h. The electromagnetic field was applied in the same manner as the MTT assay. The live and dead cells were monitored using a fluorescent microscope (Nikon BioSTation IMQ, Tokyo, Japan).

Confocal microscopy: For the mitochondrial colocalization imaging of nano-transducers, McA-RH7777 cells were treated with 150 μg/mL of RITC-labeled nano-transducers for 24 h. Intracellular mitochondria were stained with MitoTracker (Thermo Fisher, Waltham, MA, USA) according to the manufacturer's instructions. The cells were then fixed with 4% paraformaldehyde for 10 min at 25 °C and observed using a confocal microscope (Nikon A1 confocal microscope, Tokyo, Japan). For the quantitation of mitophagy, the cells were transiently transfected with the mitochondria-targeted fluorescent protein Keima (mt-Keima)

plasmid (pLVX-mtKeima)[60] and treated with nano-transducers in the presence or absence of magnetic fields. The fluorescence signal of mt-Keima was imaged using confocal microscopy with two sequential excitation lasers (458 and 561 nm, respectively). The mt-Keima fluorescence signal was measured at the 458 nm excitation wavelength in green and the 561nm laser in red. mt-Keima, a pH-sensitive fluorescent protein that is relatively resistant to lysosomal degradation, has a mitochondrial targeting sequence of cytochrome c oxidase subunit VIII, directed to the mitochondrial matrix.[61, 62] mt-Keima exhibits an excitation peak at 440 nm when the pH of the normal mitochondrial matrix is 8.0. Damaged mitochondria are in lysosomes during the mitophagy process (pH 4.5), showing a change to the 586 nm excitation peak owing to the acidic environment of the lysosome.[61] This change in mt-Keima from 440 to 586 nm depends on the acidic lysosomal pH conditions.

Western blot: Lysates from McA-RH7777 cells and tumor tissues were collected, and immunoblotting was performed as described in a previous report.[63] Cell and mitochondrial lysates were collected and immunoblotted using antibodies directed against TOM 20 (Santa Cruz), PINK1 (Cell Signaling), Parkin (Cell Signaling), p62 (Cell Signaling), LC3 (Cell Signaling), and GAPDH (Cell Signaling). The protein bands were enhanced and visualized by luminol-based detection using ECL western blotting Detection Reagent (GE Healthcare Bio-Sciences, Pittsburgh, PA, USA) and quantified using ImageJ software (NIH, Bethesda, MD, USA).

Quantitative PCR-based mtDNA damage assay: Nuclear and mtDNA damage was assessed by qPCR as previously described.[64] Briefly, genomic DNA was extracted using the QIAamp DNA Mini Kit (Qiagen, Gaithersburg, MD, USA) according to the manufacturer's protocol. PCR was performed using Ex-Taq (Clontech, Mountain View, CA, USA) with specific primers to amplify nuclear DNA (β-globin) and a mitochondrial genomic fragment in both the short and long forms, as previously described.[64] DNA was quantified by Pico-Green (Life Technologies, Grand Island, NY, USA) using the FL600 microplate

fluorescence reader with excitation and emission wavelengths of 485 nm and 530 nm, respectively. The data obtained from the mitochondrial small fragment were used to normalize the results of the mitochondrial long fragment. The number of mitochondrial lesions was calculated using the following equation: D = (1 – 2-(Δlong-Δshort)) × 10,000 (bp)/size of the long fragment (bp).

Apoptosis assay: Apoptosis was measured using histone-associated DNA fragmentation (mono- and oligonucleosomes) Cell Death Detection ELISAPLUS kit (Sigma-Aldrich, St Louis, MO, USA) as previously described using the manufacturer's protocol.[64]

Bio-TEM observation: TEM observation was performed to confirm the mitochondrial target of the nano-transducers. The nano-transducers (150 μg/mL) were treated with the McA-RH7777 cells and incubated for 4 or 24 h. The cells were fixed and dehydrated using graded ethanol. Finally, the dehydrated cells were embedded in an Epon 812 resin, which was sectioned using a microtome and observed by TEM (FEI Tecnai Spirit G2, Hillsboro, OR, USA).

Animal model: All animal procedures were performed in accordance with the Guidelines for Care and Use of Laboratory Animals of Northwestern University and approved by the Animal Ethics Committee of Northwestern University. The *in vivo* orthotopic HCC rat model was established using MCA-RH7777 hepatoma cells, as described in our previous study.[65] Four rats (n=4) were used in each group. Molecular biological analyses (PCR and western blot) of the collected tumor tissues were performed in the same manner as in the *in vitro* experiments.

Trans-catheterization procedures: Following a previous report, nano-transducers (0.5 mg/kg) were injected with proper hepatic artery into tumors in tumor-bearing rats.[65-67] A magnetic field (10 Oe, 2.0 Hz magnetic field frequency) was applied for 15 min at 12 h after the nano-transducers were administrated. Nano-transducers were injected in the control group, but the magnetic field was not applied. The rats were sacrificed 48 h after treatment with nanoparticles, and the tumor tissues were excised for analysis of

antitumor effects.

In vivo MRI: T_2-weighted MRI was performed before and after the injection of the nano-transducers through the IA route. MR scans were performed in axial orientations using a gradient-echo sequence with the following parameters: TR/TE, 1136/28 ms; slice thickness, 1 mm; field of view (FOV), 71 × 85 mm; 216 × 256 matrix; and respiratory triggering with an MRI-compatible small-animal gating system (Model 1025, SA Instruments, Stony Brook, NY).

Histological analysis: After treatment, the harvested tissues were fixed in 10% formalin solution. All tissue staining was performed in the core of the Mouse Histology and Phenotyping Laboratory (MHPL) of Northwestern University (USA). The fixed tissue was sectioned to a thickness of 5 μm and stained with TUNEL. All slides were analyzed using a TissueFAXS microscope (TissueGnostics GmbH, Vienna, Austria). Quantitative analysis of TUNEL-positive cells in the tissues was performed using ImageJ software (National Institutes of Health, Bethesda, MD, USA).

Statistical analysis: Each experiment was repeated at least three times and expressed as mean and standard deviation. Statistical analysis was performed using one-way analysis of variance and Student's t-test. All data were statistically analyzed using GraphPad Prism software (version 6.0; GraphPad Software, Inc., La Jolla, CA, USA).

Conflicts of interest

The authors declare no competing financial interest.

ACKNOWLEDGMENT

This work was mainly supported by grants R21CA173491, R01CA218659, and R01EB026207

from the National Cancer Institute and the National Institute of Biomedical Imaging and Bioengineering. This work was also supported by the Center for Translational Imaging and Mouse Histology and Phenotyping Laboratory at Northwestern University. This research used resources of the Advanced Photon Source, a U.S. Department of Energy (DOE) Office of Science User Facility operated for the DOE Office of Science by Argonne National Laboratory under Contract No. DE-AC02-06CH11357.

References

1. L. Bonnemay, C. Hoffmann and Z. Gueroui, *Wiley Interdisciplinary Reviews: Nanomedicine and Nanobiotechnology*, 2015, **7**, 342-354.
2. T.-H. Shin and J. Cheon, *Accounts of Chemical Research*, 2017, **50**, 567-572.
3. M. A. Wheeler, C. J. Smith, M. Ottolini, B. S. Barker, A. M. Purohit, R. M. Grippo, R. P. Gaykema, A. J. Spano, M. P. Beenhakker and S. Kucenas, *Nature neuroscience*, 2016, **19**, 756-761.
4. D. Seo, K. M. Southard, J.-w. Kim, H. J. Lee, J. Farlow, J.-u. Lee, D. B. Litt, T. Haas, A. P. Alivisatos and J. Cheon, *Cell*, 2016, **165**, 1507-1518.
5. F. Etoc, D. Lisse, Y. Bellaiche, J. Piehler, M. Coppey and M. Dahan, *Nature nanotechnology*, 2013, **8**, 193-198.
6. J.-H. Lee, J.-t. Jang, J.-s. Choi, S. H. Moon, S.-h. Noh, J.-w. Kim, J.-G. Kim, I.-S. Kim, K. I. Park and J. Cheon, *Nature nanotechnology*, 2011, **6**, 418-422.
7. D. Gregurec, A. W. Senko, A. Chuvilin, P. D. Reddy, A. Sankararaman, D. Rosenfeld, P.-H. Chiang, F. Garcia, I. Tafel and G. Varnavides, *ACS nano*, 2020, **14**, 8036-8045.
8. B. Yu, B. S. Choi, W. G. Li and D. H. Kim, *Nat Commun*, 2020, **11**.
9. D. H. Kim, E. A. Rozhkova, I. V. Ulasov, S. D. Bader, T. Rajh, M. S. Lesniak and V. Novosad, *Nature Materials*, 2010, **9**, 165-171.
10. W. Zhang, H. Choi, B. Yu and D.-H. Kim, *Chemical Communications*, 2020, **56**, 8810-8813.
11. G. I. Evan and K. H. Vousden, *Nature*, 2001, **411**, 342-348.
12. S. E. Weinberg and N. S. Chandel, *Nat Chem Biol*, 2015, **11**, 9-15.
13. O. Warburg, *Science*, 1956, **123**, 309-314.
14. S. Fulda, L. Galluzzi and G. Kroemer, *Nature reviews Drug discovery*, 2010, **9**, 447-464.
15. L. Galluzzi, E. Morselli, O. Kepp, I. Vitale, A. Rigoni, E. Vacchelli, M. Michaud, H. Zischka, M. Castedo and G. Kroemer, *Molecular aspects of medicine*, 2010, **31**, 1-20.
16. V. Gogvadze, S. Orrenius and B. Zhivotovsky, *Trends in cell biology*, 2008, **18**, 165-173.
17. S. Vyas, E. Zaganjor and M. C. Haigis, *Cell*, 2016, **166**, 555-566.
18. A. H. Chourasia, M. L. Boland and K. F. Macleod, *Cancer Metab*, 2015, **3**, 4.
19. P. Lu, B. J. Bruno, M. Rabenau and C. S. Lim, *J Control Release*, 2015, DOI: 10.1016/j.jconrel.2015.10.023.
20. Q. Zhang, H. Kuang, C. Chen, J. Yan, H. C. Do-Umehara, X. Y. Liu, L. Dada, K. M. Ridge, N. S.

Chandel and J. Liu, *Nat Immunol*, 2015, **16**, 458-466.
21. G. Kroemer and J. Pouyssegur, *Cancer cell*, 2008, **13**, 472-482.
22. B. Nadege, L. Patrick and R. Rodrigue, *Frontiers in bioscience*, 2009, **14**, 4015-4034.
23. Y. Tsujimoto and S. Shimizu, *Apoptosis*, 2007, **12**, 835-840.
24. S. E. Gratton, P. A. Ropp, P. D. Pohlhaus, J. C. Luft, V. J. Madden, M. E. Napier and J. M. DeSimone, *Proceedings of the National Academy of Sciences*, 2008, **105**, 11613-11618.
25. X. Duan and Y. Li, *Small*, 2013, **9**, 1521-1532.
26. J. Mohapatra, A. Mitra, H. Tyagi, D. Bahadur and M. Aslam, *Nanoscale*, 2015, **7**, 9174-9184.
27. Y. Piao, J. Kim, H. B. Na, D. Kim, J. S. Baek, M. K. Ko, J. H. Lee, M. Shokouhimehr and T. Hyeon, *Nature materials*, 2008, **7**, 242.
28. A. T. Hoye, J. E. Davoren, P. Wipf, M. P. Fink and V. E. Kagan, *Accounts of chemical research*, 2008, **41**, 87-97.
29. Y. Liu, T. Chen, C. Wu, L. Qiu, R. Hu, J. Li, S. Cansiz, L. Zhang, C. Cui and G. Zhu, *Journal of the American Chemical Society*, 2014, **136**, 12552-12555.
30. F. Etoc, C. Vicario, D. Lisse, J.-M. Siaugue, J. Piehler, M. Coppey and M. Dahan, *Nano letters*, 2015, **15**, 3487-3494.
31. S. Marrache and S. Dhar, *Proceedings of the National Academy of Sciences*, 2012, **109**, 16288-16293.
32. Y. Zhang, C. Zhang, J. Chen, L. Liu, M. Hu, J. Li and H. Bi, *ACS applied materials & interfaces*, 2017, **9**, 25152-25163.
33. X. Han, R. Su, X. Huang, Y. Wang, X. Kuang, S. Zhou and H. Liu, *Asian journal of pharmaceutical sciences*, 2019, **14**, 569-580.
34. M. P. Murphy, *Biochimica et Biophysica Acta (BBA)-Bioenergetics*, 2008, **1777**, 1028-1031.
35. M. P. Murphy and R. A. Smith, *Annu. Rev. Pharmacol. Toxicol.*, 2007, **47**, 629-656.
36. D. H. Kim, E. A. Rozhkova, I. V. Ulasov, S. D. Bader, T. Rajh, M. S. Lesniak and V. Novosad, *Nat Mater*, 2010, **9**, 165-171.
37. W. Zhang, H. Choi, B. Yu and D. H. Kim, *Chem Commun (Camb)*, 2020, **56**, 8810-8813.
38. S.-J. Kim, P. Cheresh, R. P. Jablonski, D. B. Williams and D. W. Kamp, *International journal of molecular sciences*, 2015, **16**, 21486-21519.
39. W.-X. Zong, J. D. Rabinowitz and E. White, *Molecular cell*, 2016, **61**, 667-676.
40. K. Liu, Y. Shi, X. Guo, Y. Ouyang, S. Wang, D. Liu, A. Wang, N. Li and D. Chen, *Cell death & disease*, 2014, **5**, e1078.
41. G. Ashrafi and T. Schwarz, *Cell death and differentiation*, 2013, **20**, 31.
42. R. J. Youle and D. P. Narendra, *Nature reviews. Molecular cell biology*, 2011, **12**, 9.
43. E. Hollville, R. G. Carroll, S. P. Cullen and S. J. Martin, *Molecular cell*, 2014, **55**, 451-466.
44. D. Popovic, D. Vucic and I. Dikic, *Nature medicine*, 2014, **20**, 1242-1253.
45. N. C. Chan, A. M. Salazar, A. H. Pham, M. J. Sweredoski, N. J. Kolawa, R. L. Graham, S. Hess and D. C. Chan, *Human molecular genetics*, 2011, **20**, 1726-1737.
46. N. Mizushima and B. Levine, *Nature cell biology*, 2010, **12**, 823.
47. T. Kitada, S. Asakawa, N. Hattori and H. Matsumine, *Nature*, 1998, **392**, 605.
48. M. Bueno, Y.-C. Lai, Y. Romero, J. Brands, C. M. S. Croix, C. Kamga, C. Corey, J. D. Herazo-Maya, J. Sembrat and J. S. Lee, *The Journal of clinical investigation*, 2015, **125**, 521.
49. B. Bingol, J. S. Tea, L. Phu, M. Reichelt, C. E. Bakalarski, Q. Song, O. Foreman, D. S. Kirkpatrick and M. Sheng, *Nature*, 2014, **510**, 370.
50. N. Sun, J. Yun, J. Liu, D. Malide, C. Liu, I. I. Rovira, K. M. Holmström, M. M. Fergusson, Y. H. Yoo and C. A. Combs, *Molecular cell*, 2015, **60**, 685-696.
51. R. J. Youle and D. P. Narendra, *Nat Rev Mol Cell Biol*, 2011, **12**, 9-14.

52. C. Lupfer, P. G. Thomas, P. K. Anand, P. Vogel, S. Milasta, J. Martinez, G. H. Huang, M. Green, M. Kundu, H. B. Chi, R. J. Xavier, D. R. Green, M. Lamkanfi, C. A. Dinarello, P. C. Doherty and T. D. Kanneganti, *Nature Immunology*, 2013, **14**, 480-+.
53. R. Zhou, A. S. Yazdi, P. Menu and J. Tschopp, *Nature*, 2011, **469**, 221-225.
54. A. S. Tan, J. W. Baty, L. F. Dong, A. Bezawork-Geleta, B. Endaya, J. Goodwin, M. Bajzikova, J. Kovarova, M. Peterka, B. Yan, E. A. Pesdar, M. Sobol, A. Filimonenko, S. Stuart, M. Vondrusova, K. Kluckova, K. Sachaphibulkij, J. Rohlena, P. Hozak, J. Truksa, D. Eccles, L. M. Haupt, L. R. Griffiths, J. Neuzil and M. V. Berridge, *Cell Metab*, 2015, **21**, 81-94.
55. C. Lupfer, P. G. Thomas, P. K. Anand, P. Vogel, S. Milasta, J. Martinez, G. Huang, M. Green, M. Kundu, H. Chi, R. J. Xavier, D. R. Green, M. Lamkanfi, C. A. Dinarello, P. C. Doherty and T. D. Kanneganti, *Nat Immunol*, 2013, **14**, 480-488.
56. K. Hong, C. S. Georgiades and H. G. Jean-francois, *Nature Reviews. Clinical Oncology*, 2006, **3**, 315.
57. J. F. H. Geschwind, R. Salem, B. I. Carr, M. C. Soulen, K. G. Thurston, K. A. Goin, M. van Buskirk, C. A. Roberts and J. E. Goin, *Gastroenterology*, 2004, **127**, S194-S205.
58. Y. Tan, X. Yang, S. Dai, K. Lian, L. Wen, Y. Zhu, T. Meng, X. Liu, H. Yuan and F. Hu, *Polymer Chemistry*, 2019, **10**, 512-525.
59. Y. Piao, J. Kim, H. B. Na, D. Kim, J. S. Baek, M. K. Ko, J. H. Lee, M. Shokouhimehr and T. Hyeon, *Nature materials*, 2008, **7**, 242-247.
60. N. Sun, J. Yun, J. Liu, D. Malide, C. Liu, Rovira, II, K. M. Holmstrom, M. M. Fergusson, Y. H. Yoo, C. A. Combs and T. Finkel, *Mol Cell*, 2015, **60**, 685-696.
61. N. Sun, D. Malide, J. Liu, I. I. Rovira, C. A. Combs and T. Finkel, *Nature protocols*, 2017, **12**, 1576.
62. Y. Y. Kim, J. H. Um, J. H. Yoon, H. Kim, D. Y. Lee, Y. J. Lee, H. J. Jee, Y. M. Kim, J. S. Jang and Y. G. Jang, *The FASEB Journal*, 2019, **33**, 9742-9751.
63. S.-J. Kim, P. Cheresh, R. P. Jablonski, L. Rachek, A. Yeldandi, R. Piseaux-Aillon, M. J. Ciesielski, K. Ridge, C. Gottardi and A. P. Lam, *American Journal of Physiology-Lung Cellular and Molecular Physiology*, 2020, **318**, L1084-L1096.
64. S.-J. Kim, P. Cheresh, D. Williams, Y. Cheng, K. Ridge, P. T. Schumacker, S. Weitzman, V. A. Bohr and D. W. Kamp, *Journal of Biological Chemistry*, 2014, **289**, 6165-6176.
65. J. Chen, A. Y. Sheu, W. Li, Z. Zhang, D.-H. Kim, R. J. Lewandowski, R. A. Omary, L. D. Shea and A. C. Larson, *Journal of Controlled Release*, 2014, **184**, 10-17.
66. W. Park, J. Chen, S. Cho, S.-j. Park, A. C. Larson, K. Na and D.-H. Kim, *ACS applied materials & interfaces*, 2016, **8**, 12711-12719.
67. S. K. Mouli, P. Tyler, J. L. McDevitt, A. C. Eifler, Y. Guo, J. Nicolai, R. J. Lewandowski, W. Li, D. Procissi and R. K. Ryu, *ACS nano*, 2013, **7**, 7724-7733.

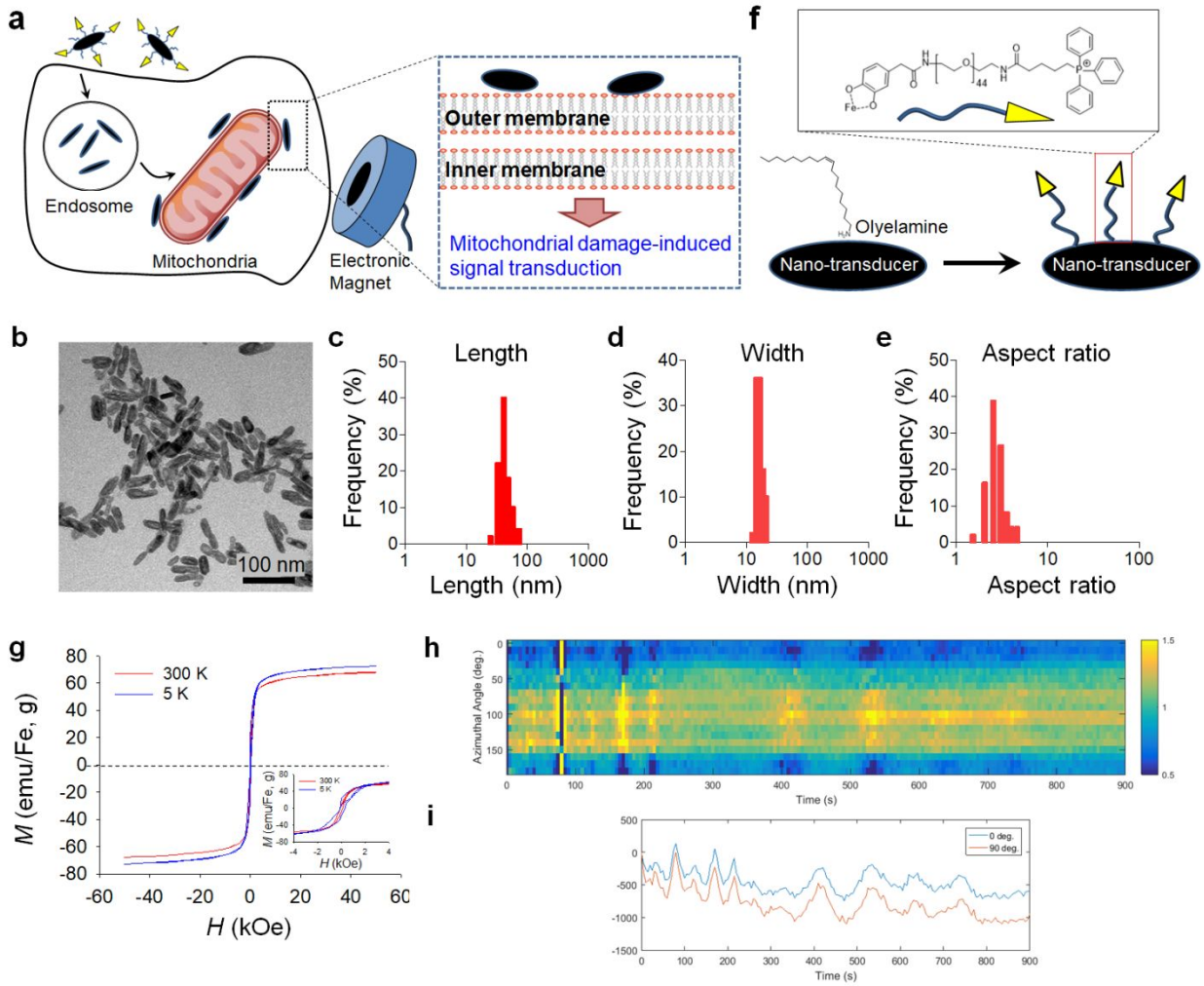

Figure 1. Mitochondria targeting magnetic nano-transducers. a, Schematic illustration of the mode of action for mitochondria targeting magnetic nano-transducers. **b**, Transmission electron microscope (TEM) image of magnetic nano-transducers (Scale bar: 100 nm). **c**, **d**, and **e**, Particle size analysis of magnetic nano-transducers: the histogram graphs indicate the **c**, length distribution, **d**, width distribution, and **e**, aspect ratio distribution of magnetic nano-transducers, respectively. **f**, Schematic illustration of mitochondria-targeting magnetic nano-transducers: The nanoparticles were functionalized with oleylamine, and mitochondria targeting polymers (*i.e.,* triphenylphosphine-polyethyleneglycol-3,4-dihydroxyphenylacetic acid (TPP-PEG-DOPAC) were conjugated to the surface of the nanoparticles. **g**, Field-dependent magnetization curves of magnetic nano-transducers at 300 K and 5 K. **h** and **i**, Small-angle X-ray scattering (SAXS) analysis of motion change of magnetic nano-transducers under an external magnetic field. **h**, Representative SAXS image of magnetic nano-transducers under external magnetic fields (10 Oe, 2.0 Hz of magnetic field frequency). **i**, SAXS signal intensity changes of magnetic nano-transducers

over time under external magnetic fields (10 Oe, 2.0 Hz of magnetic field frequency).

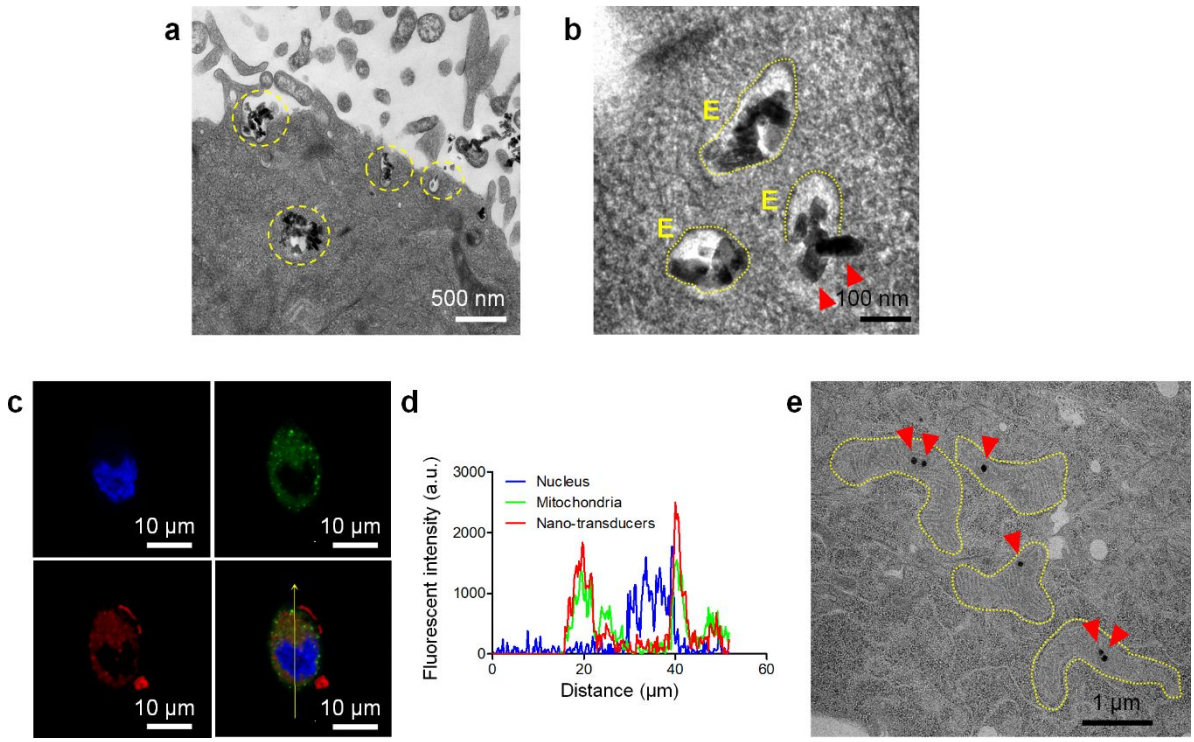

Figure 2. Mitochondrial targeting of magnetic nano-transducers in rat hepatoma cells (McA-RH7777). a and **b**, Transmission electron microscopy (TEM) images of cellular internalization of nano-transducers. **a**, TEM image in which the nano-transducers are internalized through the endocytosis mechanisms into cancer cell (at 4 h after nanoparticles treatment). **b**, TEM image capturing a scene where the nano-transducers escape from endosome (the yellow dotted line indicates the endosome, and the red triangles indicate the nano-transducers that escape from the endosome). **c**, Confocal fluorescence microscopy image of mitochondrial targeting of nano-transducers in cancer cell (blue: nucleus, green: mitochondria, red: nano-transducers, scale bar: 10 μm) at 4 h after nanoparticles treatment. **d**, Fluorescent histogram for analysis of colocalization of nucleus (blue), mitochondria (green) nano-transducers (red) signal intensities following the arrow line in the Figure 2c. **e**, TEM image of nano-transducers localized in mitochondrial membrane of cancer cell at 24 h after nanoparticles treatment (the yellow dotted line and red triangle indicate the mitochondria and nano-transducers, respectively).

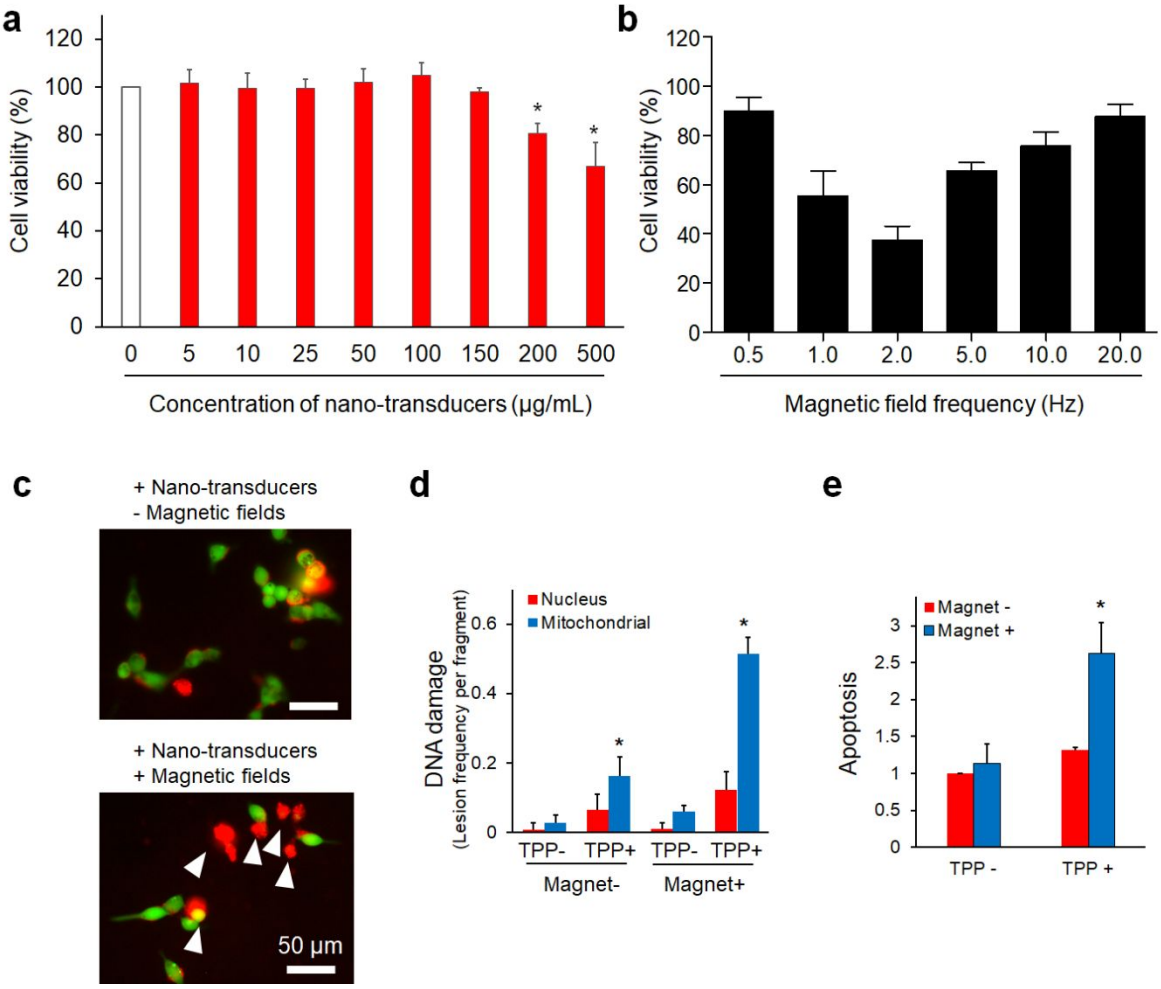

Figure 3. *In vitro* cancer cell death from mitochondrial damage caused by perturbation of magnetic nano-transducers under magnetic fields. a, *In vitro* cytotoxicity test in different concentrations of nano-transducers. **b**, *In vitro* cancer cell growth suppression of nano-transducers at various magnetic field frequency conditions. **c**, *In vitro* live and dead assay for cancer cells treated with nano-transducers (150 μg/mL) under conditions with or without magnetic fields (Scale bar: 50 μm). **d**, *In vitro* cellular nucleus and mitochondrial DNA damage assay for cancer cells treated with nano-transducers under conditions with or without magnetic fields. Mitochondrial targeting ligands (*i.e.,* TPP)-free nano-transducers, were used as a control. **e**, *In vitro* apoptosis assay for cancer cells treated with nano-transducers under conditions with or without magnetic fields.

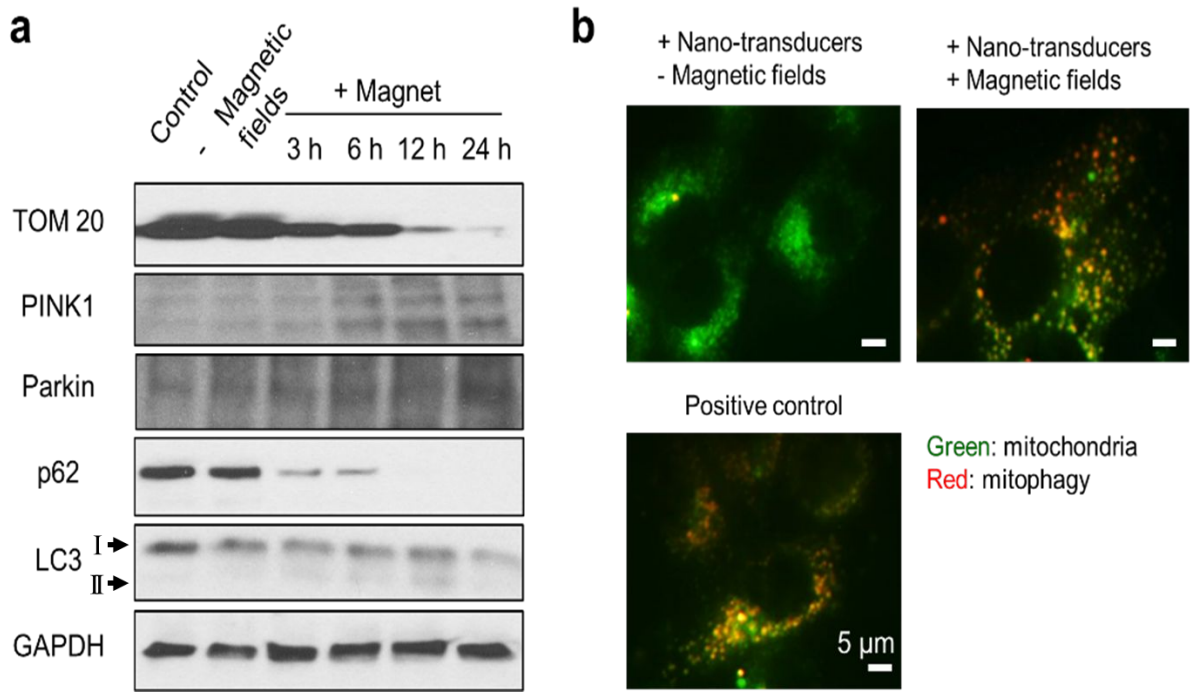

Figure 4. ***In vitro*** **mitophagy-related signal transduction from mitochondrial damage caused by perturbation of magnetic nano-transducers under magnetic fields. a**, Western blot for *in vitro* expression of proteins associated with mitophagy in cancer cells treated with nano-transducers under conditions with or without magnetic fields. **b**, *In vitro* confocal microscopy images for mt-Keima expression in cancer cells treated with nano-transducers under conditions with or without magnetic fields. The positive control group is the cancer cells that treated CCCP (30 μM) and Oligomycin (1.26 μM) to induce mitophagy.

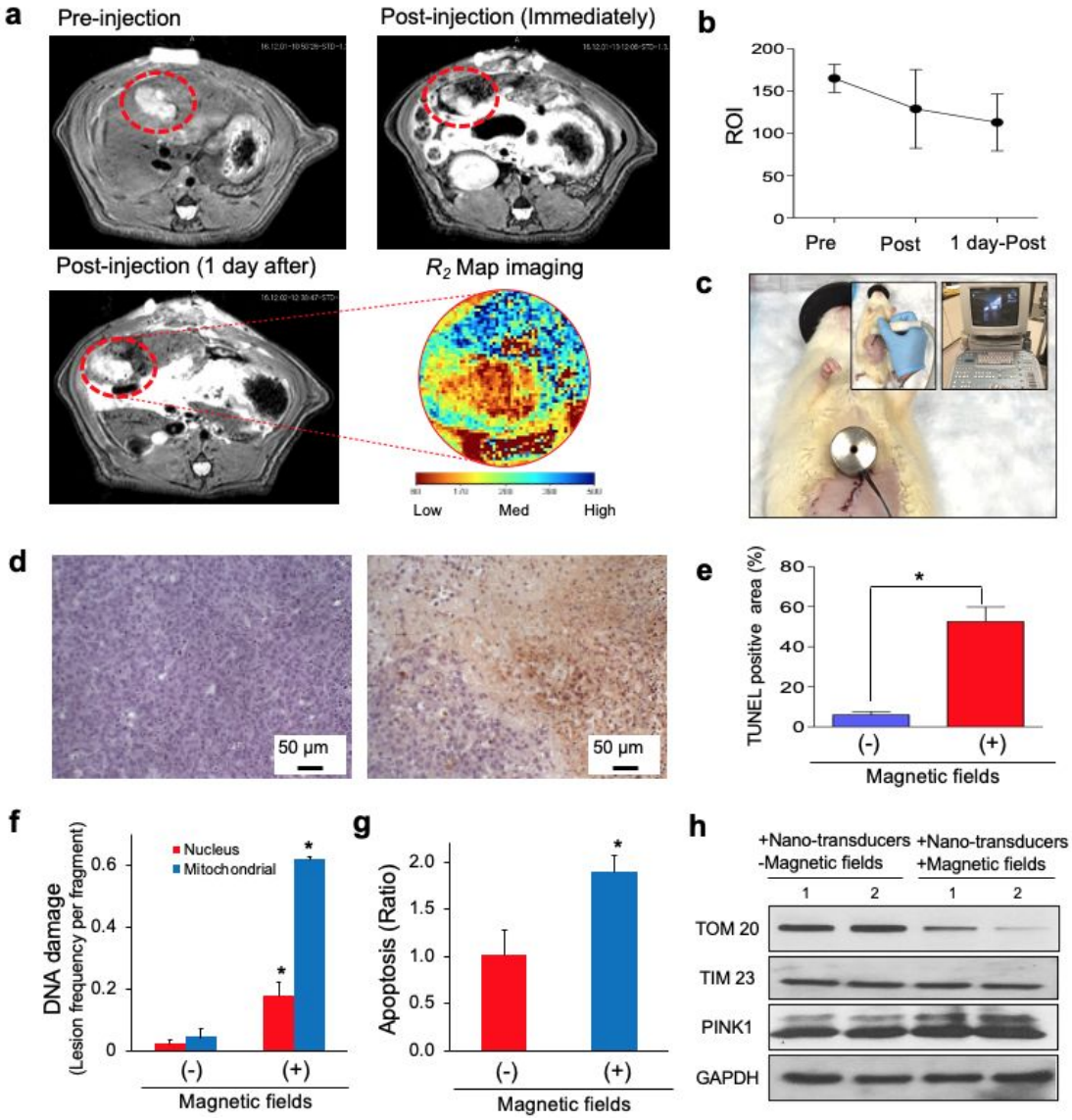

Figure 5. ***In vivo*** **cancer treatment with magnetic nano-transducers through a combination of magnetic resonance (MR) image-guided intervention and external magnetic fields in rat hepatocellular carcinoma (HCC) model. a**, *In vivo* T_2 MR image of pre- and post-injection of nano-transducers. **b**, *In vivo* T_2 MR signal (region of interest, ROI) changes in tumor tissues over time. **c**, Digital photograph of the application of an external magnet to an animal model (Inset: ultrasound imaging in the animal model). **d**, Representative optical images of the TUNEL stained tissue from (left) untreated and (right) nano-transducers with magnetic fields treatment group. **e**, Quantitative analysis of the TUNEL positive cells in the tumor tissues (n = 4, *$p < 0.05$). **f**, *In vivo* cellular nucleus and mitochondrial DNA damage assay for tumor tissues treated with nano-transducers under conditions with or without magnetic fields. **g**, *In vivo* apoptosis assay for tumor tissues treated with nano-transducers under conditions with or without magnetic fields. **h**, Western blot for *in vivo* expression of TOM 20, TIM 23, and PINK1 in the tumor tissues treated with nano-transducers under conditions with magnetic fields. The control group was only treated with nano-transducers without magnetic fields.